Effect of pH on the mobility of the herbicide MCPA in a sand-goethite column: 1D and 2D reactive transport modeling

Lippold, H.; Karimzadeh, L.; Kulenkampff, J.; Wissmeier, L.; Stuhlfauth, C.; Stoll, M.; Lippmann-Pipke, J.;

Originally published:

October 2018

Applied Geochemistry 98(2018), 345-350

DOI: https://doi.org/10.1016/j.apgeochem.2018.10.010

Accepted manuscript, printed in *Appl. Geochem.* **98** (2018) 345-350
http://dx.doi.org/10.1016/j.apgeochem.2018.10.010

Effect of pH on the mobility of the herbicide MCPA in a sand-goethite column: 1D and 2D reactive transport modeling

Holger Lippold [a,*], Lotfollah Karimzadeh [a], Johannes Kulenkampff [a], Laurin Wissmeier [b], Christin Stuhlfauth [a,c], Madeleine Stoll [a,c,d], Johanna Lippmann-Pipke [a,e]

[a] *Helmholtz-Zentrum Dresden-Rossendorf (HZDR), Institute of Resource Ecology (Research Site Leipzig), Permoserstr. 15, 04318 Leipzig, Germany*

[b] *AF-Consult Switzerland AG, Täfernstr. 26, 5405 Baden, Switzerland*

[c] *Johannes Gutenberg University Mainz, Institute for Geosciences, J.-J.-Becher-Weg 21, 55128 Mainz, Germany*

[d] *Karlsruhe Institute of Technology (KIT), Institute for Nuclear Waste Disposal, P.O. Box 3640, 76021 Karlsruhe, Germany*

[e] *Federal Institute of Geosciences and Natural Resources (BGR), Stilleweg 2, 30655 Hannover, Germany*

---

* Corresponding author.

E-mail address: h.lippold@hzdr.de (H. Lippold).

Abstract

Adsorption and transport of the herbicide 2-methyl-4-chlorophenoxyacetic acid (MCPA) in a homogeneous sand-goethite system were investigated as a function of pH. Interaction of MCPA with the solid surface was geochemically modeled according to the charge distribution multisite complexation (CD-MUSIC) approach. Based on this calibration, retardation of MCPA transport in column experiments was significantly underestimated by conventional 1D simulations.

As a new approach, Positron Emission Tomography (PET) was employed to analyze the flow field, using $^{18}F^-$ as a radiotracer. The observed heterogeneity was reproduced in 2D simulations assuming increased permeability and porosity at the periphery of the column. With this flow model, predicted retardation factors for MCPA were in agreement with the experimental data. Thus, this study demonstrates quantitatively that inconsistencies between static (batch) and dynamic (column) systems can be caused by heterogeneities in fluid flow, i.e., not necessarily by non-equilibrium conditions, which are commonly taken into account. This in turn highlights the need to consider realistic flow fields in studies of contaminant transport in natural matrices.

Keywords: CD-MUSIC model; Column experiments; Heterogeneous flow; Phenoxy acid herbicides; Positron Emission Tomography; 1D 2D transport modeling

1. Introduction

Adsorption to soil is a key process affecting plant uptake of herbicides. MCPA (2-methyl-4-chlorophenoxyacetic acid) and similar compounds are among the most widely used herbicides for controlling broad-leaved weeds under agricultural grasses. Although MCPA is applied at dosages of more than 1 kg ha^{-1}, it is not considered an environmental risk as it "disappears" rapidly in a soil environment. This is mainly attributed to its favorable structure for microbial degradation (Sandmann et al., 1988; McGhee and Burns, 1995; Jacobsen et al., 2008; Paszko, 2009), but can be due to adsorption processes as well. Decomposition is decelerated in the adsorbed state (Jensen et al., 2004). Also, low pH and low temperature increase the persistence of MCPA (Thompson et al., 1984).

Adsorption of MCPA on soils was addressed in a number of studies (Susarla et al., 1993; Shang and Arshad, 1998; Socías-Viciana et al., 1999; Haberhauer et al., 2000; Jensen et al., 2004; Sørensen et al., 2006; Jacobsen et al., 2008; Cabrera et al., 2011; Hiller et al., 2012; Waldner et al., 2012). Owing to their high pH_{PZC} values and large specific surface areas, Fe oxyhydroxides dominate the adsorption capacity of soils for phenoxy acid herbicides (Clausen and Fabricius, 2001; Thorstensen and Lode, 2001), even though they constitute only a minor part of soil minerals. Iglesias et al. (2010) and Kersten et al. (2014) investigated interaction of MCPA with a goethite surface. In both studies, adsorption as a function of pH and ionic strength was modeled using the charge distribution multisite complexation (CD-MUSIC) approach (Hiemstra and Van Riemsdijk, 1996). For parameterizing this surface complexation model, Kersten et al. (2014) derived the structures of the energetically most favorable inner-sphere and outer-sphere complexes from molecular modeling calculations based on density functional theory and molecular dynamics.

Main objective of our work was to examine as to whether surface complexation parameters, optimized for the batch system, are compatible with the flow conditions of a dynamic system.

For a variety of possible reasons, interaction constants obtained from batch studies often fail to adequately describe retention of solutes in column experiments. Non-equilibrium conditions are regarded as a major reason. A steady local equilibrium is presumed in the advection-dispersion-reaction equation. If desorption is too slow to keep up with the flow velocity, kinetic equations must be included in the reaction term.

However, another important aspect, which is often underrated, is heterogeneous flow behavior. This may occur even in simple matrices. For instance, it has been demonstrated that peripheral effects arise from the local porosity distribution in regular sphere packings (Waske et al., 2010). The interior of a column is commonly treated as a "black box". In this study, Positron Emission Tomography (PET) was applied to visualize flow processes in a column experiment. With this technique, originally developed for clinical diagnostics, radioactive tracers can be localized and quantified in opaque materials, based on the multiple coincident detection of antiparallel annihilation photons that are emitted in consequence of β^+ decays. In the authors' previous work, this non-destructive and very sensitive method was customized as "GeoPET" for 3D process monitoring in geological samples (Richter et al., 2005; Gründig et al., 2007), implementing correction modes for scattering and attenuation in dense matrices (Zakhnini et al., 2013; Kulenkampff et al., 2016a). In this way, heterogeneities in fluid flow and solute transport on the intermediate scale (mm to cm) can be visualized at high precision (Kulenkampff et al., 2008; Barth et al., 2014; Kulenkampff et al., 2016b), and effective transport parameters can be derived by inverse modeling (Lippmann-Pipke et al., 2017).

In the column experiments presented here, mobility of MCPA as a function of pH was investigated for an artificial sandy soil coated with goethite as a reactive mineral. Batch adsorption experiments were conducted to recalibrate the CD-MUSIC model from Kersten et al. (2014) for the material under study. Chemical interaction and 1D transport as a function of pH were calculated using the speciation program PHREEQC (Parkhurst and Appelo, 2013). In order to explore reasons of deviations between experimental and modeled breakthrough

curves, 2D calculations were performed by coupling PHREEQC to the finite element method software COMSOL Multiphysics® using the Java interface iCP (Nardi et al., 2014).

2. Experimental

2.1. Materials

MCPA (99%) and $NaNO_3$ were purchased from Sigma-Aldrich (Germany). Stock solutions were stored in the dark and kept no longer than 4 weeks before use. [^{3}H]H_2O with a specific activity of 37 kBq mL^{-1} was obtained from Biotrend Chemikalien (Germany).

Goethite-coated sand was prepared by mixing the following components: 1 wt.% goethite Bayferrox® 920 Z (Lanxess, Germany), grain size < 45 µm; 27 wt.% quartz silt Millisil Haltern W 11 (Quarzwerke GmbH, Germany), grain size 35 µm - 55 µm; 72 wt.% quartz sand Haltern H 33 (Quarzwerke GmbH, Germany), grain size 125 µm - 500 µm.

2.2. Batch adsorption experiments

28 mL of 10 mM $NaNO_3$ solution was added to 30 g goethite-coated sand (containing 0.3 g goethite) in 50-mL PP centrifuge tubes. After weighing the tubes, the systems were adjusted to a series of pH values (between 3.1 and 6.2) with 0.1 M HNO_3 and 0.1 M NaOH, using a SenTix 41 combination electrode (WTW, Germany). Duplicate samples were prepared for each pH. For conditioning, the systems were rotated end-over-end at 20 rpm. About 10 readjustments were necessary until the pH value was stable. The tubes were then weighed again, and the solution volume was corrected to 28 mL gravimetrically. The systems were

completed by adding 2 mL of 1.5 mM MCPA solution (in 10 mM $NaNO_3$, adjusted to pH 7.0), yielding concentrations of 0.1 mM MCPA and 1000 g L^{-1} sand/goethite (10 g L^{-1} goethite). Equilibration was performed by rotating end-over-end at 20 rpm for 24 hours. After centrifugation at 4800 rpm for 30 minutes, 3-mL samples were taken from the supernatant and were filtered through 0.45 µm PTFE syringe filters (Whatman, UK). Adsorption of MCPA to the membrane did not occur. The final pH was measured in the remaining suspensions.

To determine the adsorbed amounts, concentrations of MCPA in the supernatant samples were measured by High-Performance Liquid Chromatography (HPLC) relative to reference solutions of 0.1 mM MCPA. An HP 1100 HPLC system (Agilent, US) was used, equipped with a UV detector. Absorbance was measured at a wavelength of λ = 279 nm. Analyses were run with a Multospher® 120 RP 18-AQ-5µ column (125 mm × 4.6 mm ID), protected by a guard column with the same packing material. A 70:30 (*V*/*V*) mixture of methanol and 1 mM ammonium acetate solution (adjusted to pH 4.0) was used as eluent at a flow rate of 0.8 mL min^{-1}. The injection volume was 20 µL.

2.3. Column experiments

Self-manufactured plexiglass columns (optimized for PET measurements) were used, consisting of a cylindrical barrel (10 cm × 4 cm ID) and two end fittings with central tubing ports. Rubber seals allowed the bed length to be adjusted between 9.0 cm and 9.5 cm. Top and bottom of the column matrix were supported by fitted ETFE sieve fabric pieces (mesh size 105 µm). The columns were slurry-packed in a glove box under CO_2 atmosphere to avoid inclusion of air. Feed solutions were purged with Ar prior to use. A Jasco PU-2080 Plus HPLC pump was used for feed supply at a flow rate of 0.1 mL min^{-1}. For conditioning to the desired pH value, the columns were pre-equilibrated by passing 10-15 pore volumes of pH-

adjusted 10 mM $NaNO_3$ upward through the packed bed until a constant pH was measured in the effluent.

Hydrodynamic characteristics of the column were evaluated by applying a continuous step input of tritiated water ($[^3H]H_2O$) as a non-reactive tracer (0.3 kBq mL^{-1} in 10 mM $NaNO_3$). 3-mL fractions were collected. ^3H contents were determined with a Tri-Carb 3110 TR Liquid Scintillation Analyzer (Perkin Elmer, US) after adding Ultima Gold scintillation cocktail (Perkin Elmer, US). Hydrodynamic parameters (based on the 1D advection-dispersion equation) were fitted to the breakthrough curve by non-linear regression analysis using the program CXTFIT (Toride et al., 1995). The values are shown in Table 1.

Table 1. Hydrodynamic parameter values of the column system as determined from the breakthrough curve of $[^3H]H_2O$.

Mean pore water velocity	3.63×10^{-6} m s^{-1}
Effective porosity	0.365
Permeability	5.48×10^{-15} m^2
Dispersivity	8.67×10^{-4} m
Effective diffusion coefficient	0.30×10^{-9} m^2 s^{-1}

Breakthrough experiments with MCPA (0.1 mM in 10 mM $NaNO_3$, pH-adjusted) were carried out in a similar manner. Freshly prepared columns were used for each pH run. Concentrations of MCPA in the effluent fractions were measured by HPLC as in the batch studies.

2.4. 3D imaging by Positron Emission Tomography (PET)

A small-animal PET scanner "ClearPET" (Elysia-Raytest, Germany), customized for geological samples, was used for visualizing and quantifying radiotracer distributions inside the column. The equipment consists of a rotating gantry with 20 detector modules, each with 256 double-layered scintillation crystals on 4 photomultiplier tubes, to reach the physical resolution limit of ~ 1 mm voxel length. Image reconstruction and correction is based on the open-source STIR library (Thielemans et al., 2012). For details, the reader is referred to Kulenkampff et al. (2016a).

$^{18}F^-$ as a radiotracer (0.1 GBq) was produced at an in-house cyclotron "CYCLONE 18/9" (IBA, Belgium). 5 mL of 10 mM KF in 10 mM $NaNO_3$ was added as a carrier. This solution was injected via sample loop into a sand-goethite column, which was fed with 10 mM $NaNO_3$ at *in situ* pH (6.2) at a flow rate of 0.1 mL min^{-1}. The column was continuously operated in the field of view of the PET scanner in an upright position. ^{22}Na markers were attached to allow an exact localization of the tracer in the column.

3. Results and discussion

3.1. Adsorption of MCPA onto goethite as a function of pH

Batch studies were conducted with the sand-goethite material used in the column experiments. In preliminary tests, it was verified that the sand component is non-reactive to MCPA, as was expected in view of the low specific surface area and the low point of zero charge (pH_{PZC} ~ 2) (Kobayashi et al., 2008; Karami, 2009; Penkova et al., 2009). Accordingly, the results shown

in Fig. 1 refer to goethite. At the chosen initial concentration of 0.1 mM MCPA, adsorbed amounts are within the linear range of the adsorption isotherm (Iglesias et al., 2010).

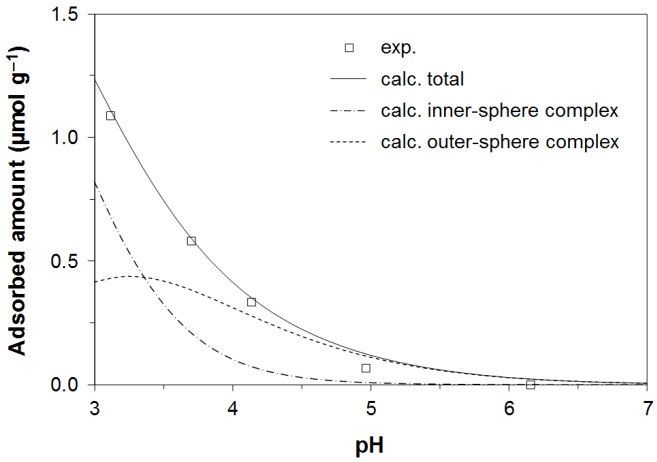

Fig. 1. Adsorption of MCPA onto goethite as a function of pH (0.1 mM MCPA, 10 mM $NaNO_3$, 10 g L^{-1} goethite). The lines show the CD-MUSIC model fit with the parameter values listed in Table 2.

Adsorption declines with increasing pH. From the viewpoint of electrostatic interaction, this may be readily explained by the progressive reduction of the positive surface charge of goethite owing to deprotonation of surface hydroxyl groups, counteracting adsorption of the anionic MCPA (Iglesias et al., 2009). Reported values of pH_{PZC} for goethite vary between 7.2 and 9.4 (Appel et al., 2003; Kosmulski et al., 2003; Ding and Pacek, 2008; Cristiano et al., 2011; Kersten et al., 2014). However, considering the absence of a significant influence of ionic strength, Kersten et al. (2014) concluded that adsorption is not primarily electrostatically driven but dominated by the formation of an inner-sphere complex. In this reaction, a carbonyl oxygen of MCPA replaces a surface hydroxyl group, which is released as a water molecule. Since this is a proton-consuming process, adsorption is promoted at low pH.

Based on energy-minimizing calculations using density functional theory in combination with statistical analysis of molecular dynamics, Kersten et al. (2014) derived detailed structural information on the surface complex. These data were used to configure the input parameters

of the CD-MUSIC surface complexation model. Besides the monodentate inner-sphere complex, a physisorbed outer-sphere complex was considered as another probable surface species. Adsorbed amounts of MCPA on goethite as a function of pH could be well described, with the outer-sphere complex being less important.

Table 2. Surface reactions and parameter values used in the CD-MUSIC model. Except for the surface reactions of MCPA, all values were adopted from Kulenkampff et al. (2018).

Surface reactions	**log *K***	**Charge distribution of adsorpt** [a]
$\equiv FeOH^{0.5-} + H^+ \rightleftharpoons FeOH_2^{0.5+}$	6.8	+1 / ±0 / ±0
$\equiv Fe_3O^{0.5-} + H^+ \rightleftharpoons Fe_3OH^{0.5+}$	6.8	+1 / ±0 / ±0
$\equiv FeOH^{0.5-} + Na^+ \rightleftharpoons FeOHNa^{0.5+}$	–0.6	±0 / ±0 / +1
$\equiv Fe_3O^{0.5-} + Na^+ \rightleftharpoons Fe_3ONa^{0.5+}$	–0.6	±0 / ±0 / +1
$\equiv FeOH^{0.5-} + H^+ + NO_3^- \rightleftharpoons FeOH_2NO_3^{0.5-}$	6.2	+1 / ±0 / –1
$\equiv Fe_3O^{0.5-} + H^+ + NO_3^- \rightleftharpoons Fe_3OHNO_3^{0.5-}$	6.2	+1 / ±0 / –1
$\equiv FeOH^{0.5-} + 2H^+ + MCPA^- \rightleftharpoons FeOH_2H(MCPA)^{0.5+}_{\text{inner-sphere}}$	11.2	+0.55 / +0.45 / ±0
$\equiv FeOH^{0.5-} + H^+ + MCPA^- \rightleftharpoons FeOHH(MCPA)^{0.5-}_{\text{outer-sphere}}$	6.4	+1 / –0.5 / –0.5
Additional parameters		
Capacitance of inner Stern layer (0- to 1-plane)	0.97 F m^{-2}	
Capacitance of outer Stern layer (1- to 2-plane)	0.93 F m^{-2}	
Specific surface area	90 m^2 g^{-1}	
Site density	3×10^{18} m^{-2}	

[a] Charges allocated to 0-plane / 1-plane / 2-plane of the Stern layer.

Compared to the study by Kersten et al. (2014), where freshly prepared goethite was used, adsorbed amounts for the commercial product used in this work were considerably lower (by a factor of ~ 50 at pH 3.1). This is partly due to a decrease in the specific surface area on ageing (Waychunas et al., 2005). Furthermore, the pH_{PZC} was reported to be very low (Kulenkampff et al., 2018). For modeling, most parameter values were taken from the latter

study, where the CD-MUSIC model from Kersten et al. (2014) was adapted to the industrial goethite material under investigation, taking the low pH_{PZC} into account. Only the interaction constants for MCPA were readjusted to describe our data. The complete parameter set is listed in Table 2. The speciation software PHREEQC (version 3) was used to calculate the concentrations of the MCPA surface species as a function of pH. The results are included in Fig. 1.

3.2. Transport of MCPA in a sand-goethite matrix at variable pH: 1D modeling

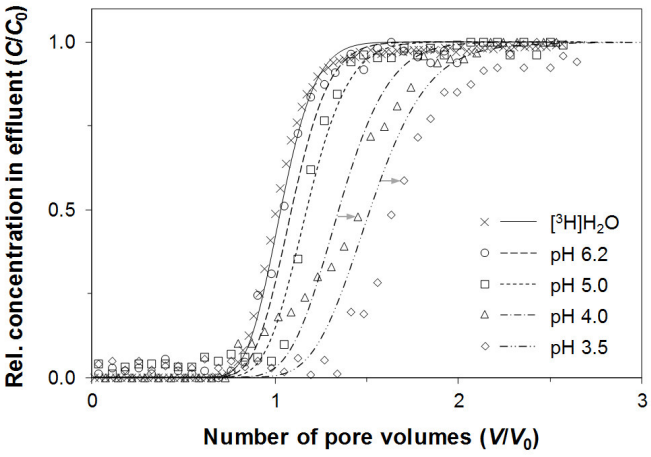

Fig. 2. Breakthrough curves for MCPA at different pH values, obtained in column experiments with goethite-coated sand (0.1 mM MCPA, 10 mM $NaNO_3$). The lines represent 1D model calculations obtained with the hydrodynamic and CD-MUSIC parameter values from Tables 1 and 2, respectively.

In Fig. 2, breakthrough curves for MCPA at 4 different pH values are shown along with the breakthrough curve for the non-reactive tracer $[^3H]H_2O$. The influence of pH on the affinity of MCPA to the goethite surface is reflected by corresponding differences in retardation. Breakthrough at pH 3.5 culminates after passage of 1.7 pore volumes, while breakthrough at pH 6.2 virtually coincides with the breakthrough of $[^3H]H_2O$. Given the dominating

adsorption capacity of Fe oxyhydroxides in soil, it can be concluded that the short half-life of MCPA as a pesticide is not "pretended" by adsorptive immobilization but is clearly attributable to biodegradation.

With the hydrodynamic parameter values derived from the breakthrough curve of $[^3H]H_2O$ (Table 1) and the chemical interaction parameter values optimized for the batch system (Table 2), the breakthrough curves of MCPA were modeled according to the 1D advection-dispersion-reaction equation

$$R\frac{\partial C}{\partial t} = D\frac{\partial^2 C}{\partial z^2} - v\frac{\partial C}{\partial z} \quad (1)$$

where C is the solute concentration, t is time, z is the longitudinal position and v is the pore water velocity. The hydrodynamic dispersion coefficient D is given by

$$D = D_e + \alpha v\theta \quad (2)$$

where D_e is the effective molecular diffusion coefficient, α is the dispersivity and θ is the porosity. For the retardation factor R, the following relation holds:

$$R = 1 + \frac{\rho K_D}{\theta} \quad (3)$$

In this equation, ρ denotes the bulk density of the solid matrix and K_D is the solute partition coefficient between solid surface and aqueous phase, here given by the CD-MUSIC surface complexation model.

The 1D simulations were performed using the explicit finite difference scheme implemented in the PHREEQC program. For discretization, the column was partitioned into 50 segments. As can be seen from Fig. 2, the breakthrough curves in the range of low adsorption (pH 6.2 and pH 5.0) are well reproduced, whereas retardation at the lower pH values is markedly underestimated.

3.3. Peripheral flow: Evidence and 2D modeling

By modeling breakthrough curves in only one dimension, any lateral effects are not accommodated. To shed light on the actual, spatial characteristics of the flow process inside the column, we investigated tracer distributions by means of Positron Emission Tomography (PET). Figure 3a shows a section view of the flow pattern of the PET tracer [^{18}F]F^{-} after pulse injection. The distribution deviates drastically from the expected flow profile for this geometry. Instead, we observe preferential flow in the peripheral zone of the column, even though it was very carefully packed.

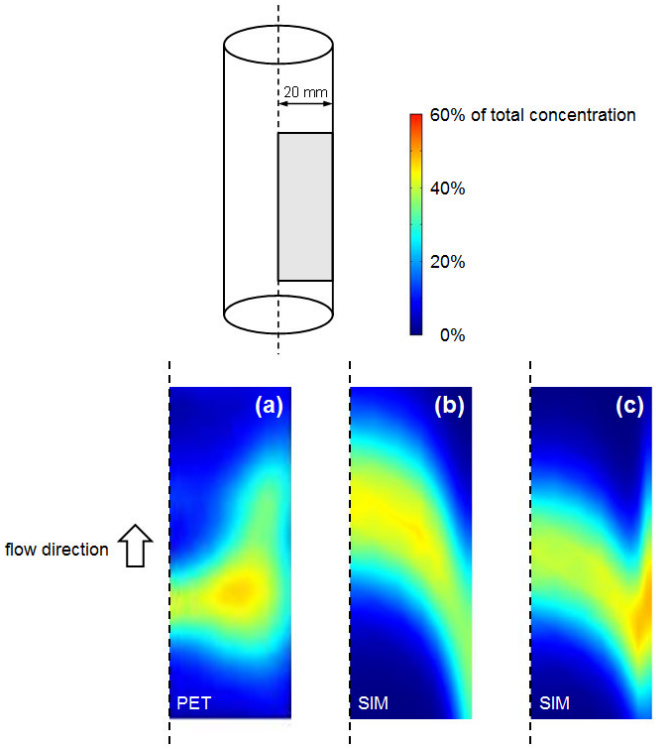

Fig. 3. Half longitudinal section view of a [^{18}F]F^{-} injection pulse (5 mL 10 mM [^{18}F]KF) in the sand-goethite column. (a) PET image, (b) result of 2D transport modeling assuming a homogeneous distribution of porosity and permeability (parameter values from Table 1), (c) result of 2D transport modeling assuming a 1-mm peripheral zone (right-hand edge) with increased porosity (0.6) and permeability (22×10^{-15} m^2).

To regard the spatial tracer distribution, transport calculations were performed with a pseudo-3D flow model (2D with rotational symmetry), considering the geometry of the column. For three spatial dimensions, the advection-dispersion-reaction equation takes the form

$$R\frac{\partial(\theta C)}{\partial t} = \nabla(\mathbf{D}\theta\nabla C) - \mathbf{u}\nabla C \tag{4}$$

with **D** denoting the hydrodynamic dispersion tensor and **u** denoting the Darcy velocity vector. (∇ is the del operator.) Note that pore water velocity v and Darcy velocity u are related by the porosity θ:

$$u = v\theta \tag{5}$$

The hydrodynamic dispersion tensor **D** is given by

$$\mathbf{D} = \begin{pmatrix} D_\mathrm{T} & 0 & 0 \\ 0 & D_\mathrm{T} & 0 \\ 0 & 0 & D_\mathrm{L} \end{pmatrix} \tag{6}$$

with the transverse and longitudinal hydrodynamic dispersion coefficients D_T and D_L, respectively:

$$D_\mathrm{T} = D_\mathrm{e} + \alpha_\mathrm{T} u \tag{7a}$$

$$D_\mathrm{L} = D_\mathrm{e} + \alpha_\mathrm{L} u \tag{7b}$$

It is assumed that the transverse dispersivity α_T amounts to one tenth of the longitudinal dispersivity α_L.

The Darcy velocity vector **u** in Eq. (4) is determined by the fluid pressure gradient ∇p in flow direction, according to Darcy's law

$$\mathbf{u} = -\frac{\kappa}{\mu}\nabla p \tag{8}$$

where κ is the permeability and μ is the dynamic viscosity of the fluid.

The finite element method software COMSOL Multiphysics® (version 5.3) was used for this modeling. Figure 3b shows the calculated tracer distribution at V/V_0 = 0.5 for a central injection source assuming homogeneous porosity and permeability throughout the column. It

is obvious that the actual flow profile (Fig. 3a) is not adequately described in this way. To align the simulation results with the PET imaging results by a straightforward parameter variation, a peripheral zone with a radial thickness of 1 mm was defined where the values of porosity and permeability were gradually increased. As can be seen in Fig. 3c, the essential characteristics of the flow pattern can be roughly reproduced with peripheral values for porosity and permeability exceeding the bulk values by factors of 2 and 4, respectively. We abstained from fitting the observed 2D distribution in more detail to keep the model as simple as possible.

With the same homogeneous and heterogeneous 2D flow models, plus the CD-MUSIC model calibrated for the batch system, reactive transport of MCPA at pH 3.5 was calculated using the interface software iCP, which connects the codes COMSOL Multiphysics® and PHREEQC. The results are shown in Fig. 4.

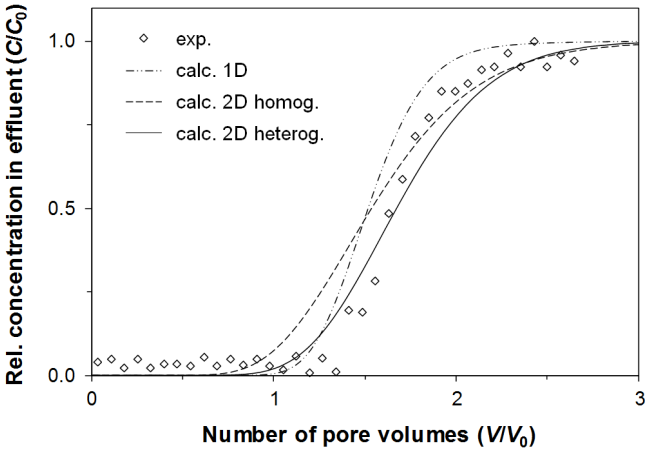

Fig. 4. Experimental and modeled breakthrough curves for MCPA at pH 3.5. The 1D calculation (cf. Fig. 2) considers longitudinal dispersion only. The homogeneous and heterogeneous 2D calculations are based on the flow models applied in Figs. 3b and 3c, respectively. Chemical interaction is described by the CD-MUSIC model with parameter values optimized for the batch system (Fig. 1).

The slopes of the breakthrough curves obtained with the 2D models are less steep as compared to the 1D model, which is explained by the consideration of lateral dispersion in addition to longitudinal dispersion. With a homogeneous distribution of porosity and permeability, retardation is underestimated as with the 1D model. However, if the peripheral flow effect is taken into account by a heterogeneous arrangement of θ und κ as in Fig. 3c (identical values), the calculated breakthrough curve is shifted to longer retention times. The retardation factor (inflection point) now almost exactly agrees with the experimental result. This applies likewise to the breakthrough curve for pH 4.0 (Supplementary Material, Fig. A.1). Note that there are not any parameter adjustments regarding MCPA transport. The shift to later breakthrough can be understood from a comparison of the simulated flow fields, shown in the Supplementary Material, Fig. A.2.

4. Summary and conclusions

In accordance with its adsorption behavior, mobility of MCPA in a flow system with goethite as a reactive matrix component proved to be dependent on the pH value. At circumneutral conditions as encountered in most agricultural soils, transport of MCPA is nearly unretarded. From this viewpoint, plant uptake and microbial availability can be assumed to be largely unaffected. For a more general evaluation of MCPA mobility in soil, other potentially reactive components such as aluminum oxides and humic matter must of course be included in the consideration, particularly their combined effects in mixtures.

A major focus of this work was set on the explanation of discrepancies in quantitative results obtained from batch and column experiments – a general issue in reactive transport modeling. Surface complexation parameters, adjusted to adsorption in batch systems as a function of pH, failed to describe the increase in retention at low pH under flow conditions. Underestimations

as found here are commonly explained by slow desorption. While this is not excluded in the present case, this study provides quantitative evidence that inconsistencies between static and dynamic systems are not necessarily due to non-equilibrium conditions but can be caused by heterogeneous (e.g. peripheral) flow as well. This conclusion can be drawn even though 2D simulation and breakthrough fit are not perfect within the bounds of the simple model.

Positron Emission Tomography was demonstrated to be a key technique for the analysis of heterogeneous flow fields, providing a basis for quantitative assessments of implications with respect to migration speeds also in subsurface environments. Disregarding this effect impairs the meaningfulness of interaction parameters in transport prognoses. Fluid flow in geological matrices like porous or fractured rock is in need of investigation.

Acknowledgements

This work was funded by the German Research Foundation (DFG), support code LI872/5, within the priority program SPP 1315 “Biogeochemical Interfaces in Soil”. The authors would like to thank T. Ritschel (Friedrich Schiller University Jena) for providing the sand-goethite material and K. Franke (HZDR) for the production of $^{18}F^-$.

Appendix A. Supplementary data

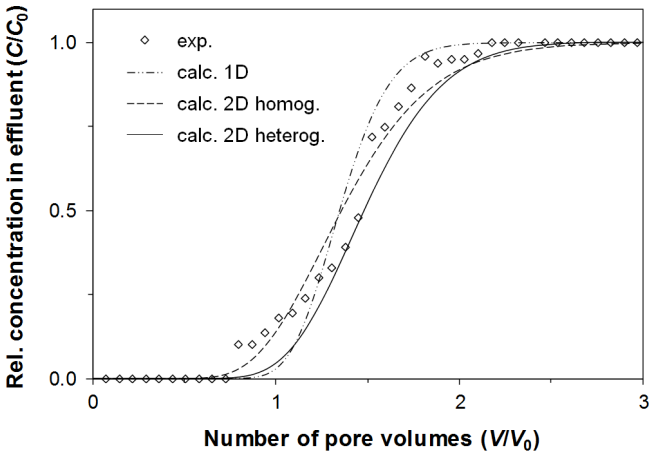

Fig. A.1. Experimental and modeled breakthrough curves for MCPA at pH 4.0, corresponding to the results for pH 3.5 shown in Fig. 4.

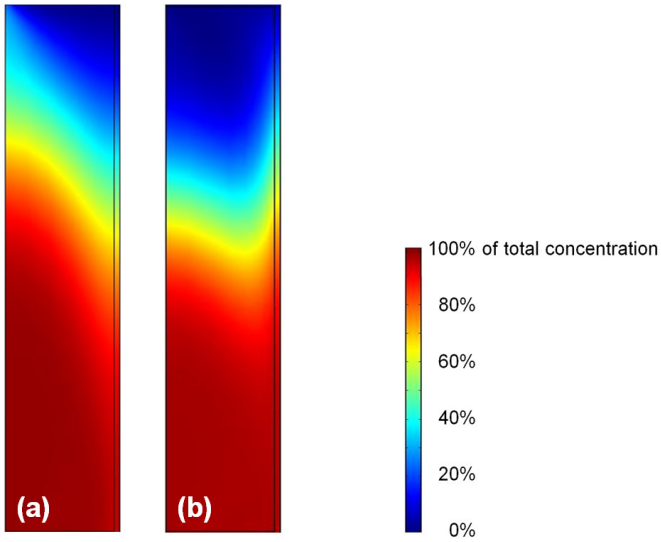

Fig. A.2. Half longitudinal section view of the distribution of MCPA in the column for equal times at beginning breakthrough (V/V_0 = 0.97), corresponding to the 2D simulations in Fig. 4 with homogeneous (a) and heterogeneous (b) flow model.

References

Appel, C., Ma, L.Q., Rhue, R.D., Kennelley, E., 2003. Point of zero charge determination in soils and minerals via traditional methods and detection of electroacoustic mobility. Geoderma 113, 77–93.

Barth, T., Ludwig, M., Kulenkampff, J., Gründig, M., Franke, K., Lippmann-Pipke, J., Hampel, U., 2014. Positron emission tomography in pebble beds. Part 1: Liquid particle deposition. Nucl. Eng. Des. 267, 218–226.

Cabrera, A., Cox, L., Spokas, K.A., Celis, R., Hermosín, M.C., Cornejo, J., Koskinen, W.C., 2011. Comparative sorption and leaching study of the herbicides fluometuron and 4-chloro-2-methylphenoxyacetic acid (MCPA) in a soil amended with biochars and other sorbents. J. Agr. Food Chem. 59, 12550–12560.

Clausen, L., Fabricius, I., 2001. Atrazine, isoproturon, mecoprop, 2,4-D, and bentazone adsorption onto iron oxides. J. Environ. Qual. 30, 858–869.

Cristiano, E., Hu, Y.-J., Siegfried, M., Kaplan, D., Nitsche, H., 2011. A comparison of point of zero charge measurement methodology. Clay Clay Miner. 59, 107–115.

Ding, P., Pacek, A.W., 2008. De-agglomeration of goethite nano-particles using ultrasonic comminution device. Powder Technol. 187, 1–10.

Gründig, M., Richter, M., Seese, A., Sabri, O., 2007. Tomographic radiotracer studies of the spatial distribution of heterogeneous geochemical transport processes. Appl. Geochem. 22, 2334–2343.

Haberhauer, G., Pfeiffer, L., Gerzabek, M.H., 2000. Influence of molecular structure on sorption of phenoxyalkanoic herbicides on soil and its particle size fractions. J. Agr. Food Chem. 48, 3722–3727.

Hiemstra, T., Van Riemsdijk, W.H., 1996. A surface structural approach to ion adsorption: The charge distribution (CD) model. J. Colloid Interf. Sci. 179, 488–508.

Hiller, E., Tatarková, V., Šimonovičová, A., Bartal, M., 2012. Sorption, desorption, and degradation of (4-chloro-2-methylphenoxy)acetic acid in representative soils of the Danubian Lowland, Slovakia. Chemosphere 87, 437–444.

Iglesias, A., López, R., Gondar, D., Antelo, J., Fiol, S., Arce, F., 2009. Effect of pH and ionic strength on the binding of paraquat and MCPA by soil fulvic and humic acids. Chemosphere 76, 107–113.

Iglesias, A., López, R., Gondar, D., Antelo, J., Fiol, S., Arce, F., 2010. Adsorption of MCPA on goethite and humic acid-coated goethite. Chemosphere 78, 1403–1408.

Jacobsen, C.S., van der Keur, P., Iversen, B.V., Rosenberg, P., Barlebo, H.C., Torp, S., Vosgerau, H., Juhler, R.K., Ernstsen, V., Rasmussen, J., Brinch, U.C., Jacobsen, O.H., 2008. Variation of MCPA, metribuzine, methyltriazine-amine and glyphosate degradation, sorption, mineralization and leaching in different soil horizons. Environ. Pollut. 156, 794–802.

Jensen, P.H., Hansen, H.C.B., Rasmussen, J., Jacobsen, O.S., 2004. Sorption-controlled degradation kinetics of MCPA in soil. Environ. Sci. Technol. 38, 6662–6668.

Karami, A., 2009. Study on modification of colloidal silica surface with magnesium ions. J. Colloid Interf. Sci. 331, 379–383.

Kersten, M., Tunega, D., Georgieva, I., Vlasova, N., Branscheid, R., 2014. Adsorption of the herbicide 4-chloro-2-methylphenoxyacetic acid (MCPA) by goethite. Environ. Sci. Technol. 48, 11803–11810.

Kobayashi, Y., Imai, J., Nagao, D., Konno, M., 2008. Fabrication of Eu-coated silica particles by homogeneous precipitation method. Colloids Surf. A 326, 109–114.

Kosmulski, M., Maczka, E., Jartych, E., Rosenholm, J.B., 2003. Synthesis and characterization of goethite and goethite–hematite composite: experimental study and literature survey. Adv. Colloid Interfac. 103, 57–76.

Kulenkampff, J., Gründig, M., Richter, M., Enzmann, F., 2008. Evaluation of positron-emission-tomography for visualisation of migration processes in geomaterials. Phys. Chem. Earth 33, 937–942.

Kulenkampff, J., Gründig, M., Zakhnini, A., Lippmann-Pipke, J., 2016a. Geoscientific process monitoring with positron emission tomography (GeoPET). Solid Earth 7, 1217–1231.

Kulenkampff, J., Stoll, M., Gründig, M., Mansel, A., Lippmann-Pipke, J., Kersten, M., 2018. Time-lapse 3D imaging by positron emission tomography of Cu mobilized in a soil column by the herbicide MCPA. Sci. Rep.-UK 8, 7091.

Kulenkampff, J., Zakhnini, A., Gründig, M., Lippmann-Pipke, J., 2016b. Quantitative experimental monitoring of molecular diffusion in clay with positron emission tomography. Solid Earth 7, 1207–1215.

Lippmann-Pipke, J., Gerasch, R., Schikora, J., Kulenkampff, J., 2017. Benchmarking PET for geoscientific applications: 3D quantitative diffusion coefficient determination in clay rock. Comput. Geosci. 101, 21–27.

McGhee, I., Burns, R.G., 1995. Biodegradation of 2,4-dichlorophenoxyacetic acid (2,4-D) and 2-methyl-4-chlorophenoxyacetic acid (MCPA) in contaminated soil. Appl. Soil Ecol. 2, 143–154.

Nardi, A., Idiart, A., Trinchero, P., de Vries, L.M., Molinero, J., 2014. Interface COMSOL-PHREEQC (iCP), an efficient numerical framework for the solution of coupled multiphysics and geochemistry. Comput. Geosci. 69, 10–21.

Parkhurst, D.L., Appelo, C.A.J., 2013. Description of input and examples for PHREEQC version 3: a computer program for speciation, batch-reaction, one-dimensional transport, and inverse geochemical calculations. U.S. Geological Survey Techniques and Methods, Book 6, Chapter A43, Denver, CO.

Paszko, T., 2009. Degradation of MCPA in soil horizons of Polish agricultural soils. Pol. J. Environ. Stud. 18, 1083–1091.

Penkova, A., Martínez Blanes, J.M., Cruz, S.A., Centeno, M.A., Hadjiivanov, K., Odriozola, J.A., 2009. Gold nanoparticles on silica monospheres modified by amino groups. Micropor. Mesopor. Mat. 117, 530–534.

Richter, M., Gründig, M., Zieger, K., Seese, A., Sabri, O., 2005. Positron emission tomography for modelling of geochemical transport processes in clay. Radiochim. Acta 93, 643–651.

Sandmann, E.R.I.C., Loos, M.A., van Dyk, L.P., 1988. The microbial degradation of 2,4-dichlorophenoxyacetic acid in soil. Rev. Environ. Contam. T. 101, 1–53.

Shang, C., Arshad, M.A., 1998. Sorption of clopyralid, dicamba and MCPA by two soils with conventional and no-till management. Can. J. Soil Sci. 78, 181–186.

Socías-Viciana, M.M., Fernández-Pérez, M., Villafranca-Sánchez, M., González-Pradas, E., Flores-Céspedes, F., 1999. Sorption and leaching of atrazine and MCPA in natural and peat-amended calcareous soils from Spain. J. Agr. Food Chem. 47, 1236–1241.

Sørensen, S.R., Schultz, A., Jacobsen, O.S., Aamand, J., 2006. Sorption, desorption and mineralisation of the herbicides glyphosate and MCPA in samples from two Danish soil and subsurface profiles. Environ. Pollut. 141, 184–194.

Susarla, S., Bhaskar, G.V., Bhamidimarri, S.M.R., 1993. Adsorption-desorption characteristics of some phenoxyacettc acids and chlorophenols in a volcanic soil I. Equilibrium and kinetics. Environ. Technol. 14, 159–166.

Thielemans, K., Tsoumpas, C., Mustafovic, S., Beisel, T., Aguiar, P., Dikaios, N., Jacobson, M.W., 2012. STIR: software for tomographic image reconstruction release 2. Phys. Med. Biol. 57, 867–883.

Thompson, D.G., Stephenson, G.R., Solomon, K.R., Skepasts, A.V., 1984. Persistence of (2,4-dichlorophenoxy)acetic acid and 2(2,4-dichlorophenoxy)propionic acid in

agricultural and forest soils of Northern and Southern Ontario. J. Agr. Food Chem. 32, 578–581.

Thorstensen, C.W., Lode, O., 2001. Laboratory degradation studies of bentazone, dichlorprop, MCPA, and propiconazole in Norwegian soils. J. Environ. Qual. 30, 947–953.

Toride, N., Leij, F.J., Van Genuchten, M.T., 1995. The CXTFIT code for estimating transport parameters from laboratory or field tracer experiments, version 2.0. U. S. Dept. of Agriculture, Riverside, CA.

Waldner, G., Friesl-Hanl, W., Haberhauer, G., Gerzabek, M.H., 2012. Differences in sorption behavior of the herbicide 4-chloro-2-methylphenoxyacetic acid on artificial soils as a function of soil pre-aging. J. Soils Sediments 12, 1292–1298.

Waske, A., Heiland, M., Beckmann, F., Odenbach, S., 2010. Absorption edge X-ray tomography for the analysis of particle deposition in packed bed filters. AIP Conf. Proc. 1254, 187–192.

Waychunas, G.A., Kim, C.S., Banfield, J.F., 2005. Nanoparticulate iron oxide minerals in soils and sediments: unique properties and contaminant scavenging mechanisms. J. Nanopart. Res. 7, 409–433.

Zakhnini, A., Kulenkampff, J., Sauerzapf, S., Pietrzyk, U., Lippmann-Pipke, J., 2013. Monte Carlo simulations of GeoPET experiments: 3D images of tracer distributions (^{18}F, ^{124}I and ^{58}Co) in Opalinus clay, anhydrite and quartz. Comput. Geosci. 57, 183–196.